

Single-step Chemical Vapor Deposition of Methyl Ammonium Lead Halide Perovskite for p-i-n Solar Cells

*Dmitry S. Muratov*¹, Lev Luchnikov¹, Danila Saranin¹, Artur Ishteev^{1,3}, Vladislav Kurichenko²,
Evgeniy Kolesnikov¹, Denis V. Kuznetsov² and Aldo Di Carlo⁴*

¹L.A.S.E. – Laboratory for Advanced Solar Energy, National University of Science and
Technology “MISiS”, Leninskiy prospect 6, Moscow, 119049, Russia

²Department of Functional NanoSystems and High-Temperature Materials, National University
of Science and Technology “MISiS”, Leninskiy prospect 4, Moscow, 119049, Russia

³N.N. Semenov Federal Research Center for Chemical Physics, Russian Academy of Sciences,
Kosygina st. 4, Moscow, 119991, Russia

⁴CHOSE – Centre for Hybrid and Organic Solar Energy, Department of Electronic Engineering,
University of Rome Tor Vergata, via del Politecnico 1, Rome, 00133, Italy

*Corresponding Author E-mail Address: muratov@misis.ru

KEYWORDS: Chemical Vapor Deposition, Chemical properties of optoelectronic materials, Coatings, Thin-film electronics,, Energy Conversion - Photovoltaics, Perovskite Solar Cells,

Abstract

Metal halide perovskite solar cells being one of the fastest emerging technologies for renewable energy still has to become more industry friendly in a way that will allow using it for thin film modules or tandems with conventional silicon devices. The simplest way to achieve this is to use chemical vapor deposition (CVD) technique for tandem production. In this work, we show a method for a single step production of MAPbI₃ films in a simple two-zone CVD reactor from lead diacetate and methyl-ammonium iodide powders. Obtained films show highly ordered cubic MAPbI₃ phase with a thickness of 400-500 um, good photoluminescence response and absorption band edge similar to spin-coated film. We used those films to produce p-i-n solar cells with ITO/NiO/MAPbI₃/C60/Cu structure. The best cell showed negligible 0.23 % PCE right after the manufacturing but significantly improved to 5.5 % PCE after 8 hours of storage in the dark. The main limiting factor affecting the efficiency is low current density, which we attribute to non-optimized growth conditions; however, our approach is a first step to a single step CVD deposition of MAPbI₃ on any type of substrates including texturized silicon subcells for better overall efficiency.

Introduction

Metal-organic halide perovskites (HP) have shown an impressive performance leap in thin-film solar cell technology over the last 10 years. The most famous member of the HP family is the methyl-ammonium lead iodide (MAPbI₃)¹, which has been studied, characterized, and widely used for fabrication of perovskite solar cells with efficiency even exceeding the 25%². More recently

the use of multication perovskite such as CsMAFAPbI₃ or CsFAPbI₃^{3,4} with reduced bandgap permitted to increase cell efficiency and improve stability⁵. Nevertheless, single cation MA-based perovskites are still of the interest and their use in different PV applications has been considered⁶. One of the main successes of MAPbI₃ are its simple deposition process based of solution-process coating techniques such as spin-coating⁷ slot-die printing⁸, screen-printing⁹ and blade-coating techniques¹⁰. At the same time, physical deposition techniques such as thermal sublimation has been proven to be compatible with halide perovskite deposition especially when conformable coating is necessary an in the case of tandem perovskite/silicon where PSC is deposited on a texturized silicon surface¹¹. Among different physical deposition technique, the chemical vapor deposition (CVD) method is one of the most suited ad industry level and well recognized for conventional PV technology^{12,13} Most of the published research on MAPbI₃ CVD used either spin-coated PbI₂ films^{14,15} as a required preliminary step for photoactive layer production or involve thermal evaporation of PbI₂ in high-vacuum conditions¹⁶. These routes produce very good quality films but getting similar results in a single step reaction will yield a more industry friendly method ready to use in already available equipment or for silicon-perovskite tandem production. The only paper describing full CVD produced solar cell in single-step manner used an n-i-p structure with FTO/TiO₂ layer being in a hot zone of the furnace for perovskite deposition¹⁷ but the extension to the inverted structure where the HP is deposited on a hole transporting material (HTM) has not been demonstrated. Considering the importance, the p-i-n structure is gaining in the recent time, especially for the tandem perovskite/silicon¹⁸ we focus our attention in developing a single-step CVD process suitable for the p-i-n configuration. In doing this, we also take care to the thermal budget of the process considering that the HTM in p-i-n structure is typically an organic material such as PEDOT:PSS, PTAA or a Self-Assembling organic Monolayer (SAM).

Experimental

We used chemically pure 99.99% lead iodide (PbI_2) (Lanhit), lead diacetate trihydrate ($\text{Pb}(\text{CH}_3\text{COO})_2 \cdot 3\text{H}_2\text{O}$) 98% (Lenreactiv) and methylammonium iodide ($\text{CH}_3\text{NH}_3\text{I}$) (Great Cell). We used pure argon (99.9995 %) as a carrier gas with mass flow controllers in two types of quartz tubes 25 mm and 50 mm in diameter. In a typical synthesis procedure, the precursor materials are put into separate quartz boats inside a bigger quartz tube reactor with a single heated area by the tube furnace (Carbolite EST 1200) for the 25 mm tubes (**fig. 1a**). In case of separate evaporation and deposition zones (50 mm tube) we used homemade chromel heater over evaporation zone and the tube furnace for the deposition zone. Solar cells with p-i-n configuration were made on patterned glass/ITO/NiO substrates, where NiO layer is spin-coated from NiCl solution as described elsewhere¹⁹. Photoactive layer was then covered by thermally evaporated C60 at 10^{-6} Torr vacuum level. Bathocuproine interlayer was spin coated at 4000 RPMs (30s) and annealed at 50 °C (1 min) for reference devices. Copper cathode was deposited also with thermal evaporation method through shadow mask to form 0.15 cm² active area for each cell.

To analyze the structure and morphology of obtained films we used scanning electron microscopy (SEM) images obtained with Tescan Vega 3. Molecular structure was analyzed with Fourier-transform infrared (FTIR) spectrometer (Thermo Nicolet) in attenuated total reflectance mode with ZnSe crystal. Crystal structure and phase composition was analyzed by X-Ray diffraction method with XRD patterns measured on Difre instrument with Cr $K\alpha$ radiation (0.229 nm). Absorbance and photoluminescence spectra of MAPbI₃ films were measured using Shimadzu UV-Viz 1280 and Carry Eclipse spectrometer with 550 nm excitation wavelength. The

photovoltaic (PV) parameters for fabricated PSCs (open-circuit voltage - Voc, short circuit current density - Jsc, fill factor – FF, and power conversion efficiency – PCE) were calculated from the IV characteristics measured under standard conditions of 1.5 AM G light spectrum. We used Xenon arc-lamp based solar simulator (ABET 3000) with AAA grade of conformity to the reference Air Mass 1.5 Global spectrum of the terrestrial solar light (1.5 AM G standard - (ASTM) G-173). The standard power density of the incoming light (100 mW/cm²) was calibrated with certified Si- reference solar cell. The scan sweeps and the MPPT tuning measurements were performed with Keithley 2400 SMU.

Results and Discussion

We compared two types of precursors for lead sources, namely lead iodide (PbI₂) and lead diacetate (PbAc₂) with CH₃NH₃I for iodide and methyl-amine groups respectively. Lead iodide as a precursor is widely discussed in literature¹⁹ being a relatively stable reagent leaving no additional components after the formation of MAPbI₃ structure. For CVD approach, however, PbI₂ is not very convenient due to very different melting points of PbI₂ and MAI (402 °C and 270 °C, respectively)²⁰. However, beside PbI₂, formation of MAPbI₃ perovskite with cubic structure can be obtained from other precursors such as lead diacetate (PbAc₂)²¹, lead oxides²² or pure metallic lead²³. To obtain a MAPbI₃ film with a single zone CVD furnace we needed to use a precursor with similar melting and evaporation temperatures to MAI and this condition is well met by PbAc₂. We should point out that even chemically pure lead diacetate if stored in ambient conditions will eventually become lead diacetate trihydrate (Pb(CH₃COO)₂·3H₂O) which melts at 75 °C in its crystalline water and then decomposes at 200 °C . This process does not allow forming a stable MAPbI₃ structure and for this reason, PbAc₂ must be freeze dried before use to remove all the crystalline water²⁴.

Several experiments have been performed to compare the CVD growth of MAPbI₃ obtained with two types of precursors. If the CVD is performed in argon flow but without vacuum conditions, we either obtained unstable brown film which became opaque white when taken out from the furnace or MAI reacted with PbAc₂ in the crucible producing lead oxides on the tube and on the substrates. To avoid this problem a vacuum conditions (10⁻¹ mbar) were introduced combined with fixed argon flow. For the experiments with 25 mm tubes we used stable 75 sccm argon flow.

We compared both PbI₂ and PbAc₂ precursors with the same synthesis parameters such as substrate positions and gas flow to analyze the film quality, its composition, morphology and optical properties. The temperature in the hot zone of the furnace for PbAc₂ was 200 °C and for the PbI₂ 350 °C due to different melting points. The cold zone of the furnace has the temperature 50°C lower compared to the hot zone (**fig. 1a**). For PbAc₂ it drops to 150 °C and for PbI₂ to 200 °C resulting in gradual change of film composition with the length of the tube reactor. Most of the experiments were done with two substrates (12.5 mm x 25 mm) placed one after another to observe the formation of all the phases for further analysis. The first substrate from the precursor crucible along the gas flow has two different color zones: the first bright yellow film is mainly related to PbI₂ as measured by XRD while the second zone has a dark brown color that is MAPbI₃. The next substrate in most of the experiments is also of dark brown color but has different morphology and it has high excess of iodine. Scanning electron microscopy (SEM) images from the dark part of the first substrates for PbAc₂ and PbI₂ precursors are shown in **Fig. 1b** and **c**, respectively. The morphology of the film obtained from PbAc₂ has apparent cubic structure and the film itself does not have any cracks or pores. Mean grain size slightly varies from 0.45 to 0.55 μm and the film thickness is 400-500 nm as measured by stylus profilometry. The dark films obtained from PbI₂ has larger crystals and very rough surface. The grain size varies from 15 to 25 μm, but at higher

magnification (right inlet of **Fig. 1c**) we noticed small hexagonal flakes which resemble the structure of PbI_2 . To analyze the crystal structure of the film for the different zones and for the two precursor we performed X-Ray diffraction (XRD) measurements. XRD patterns are shown in **Fig. 2** together with the images of substrates.

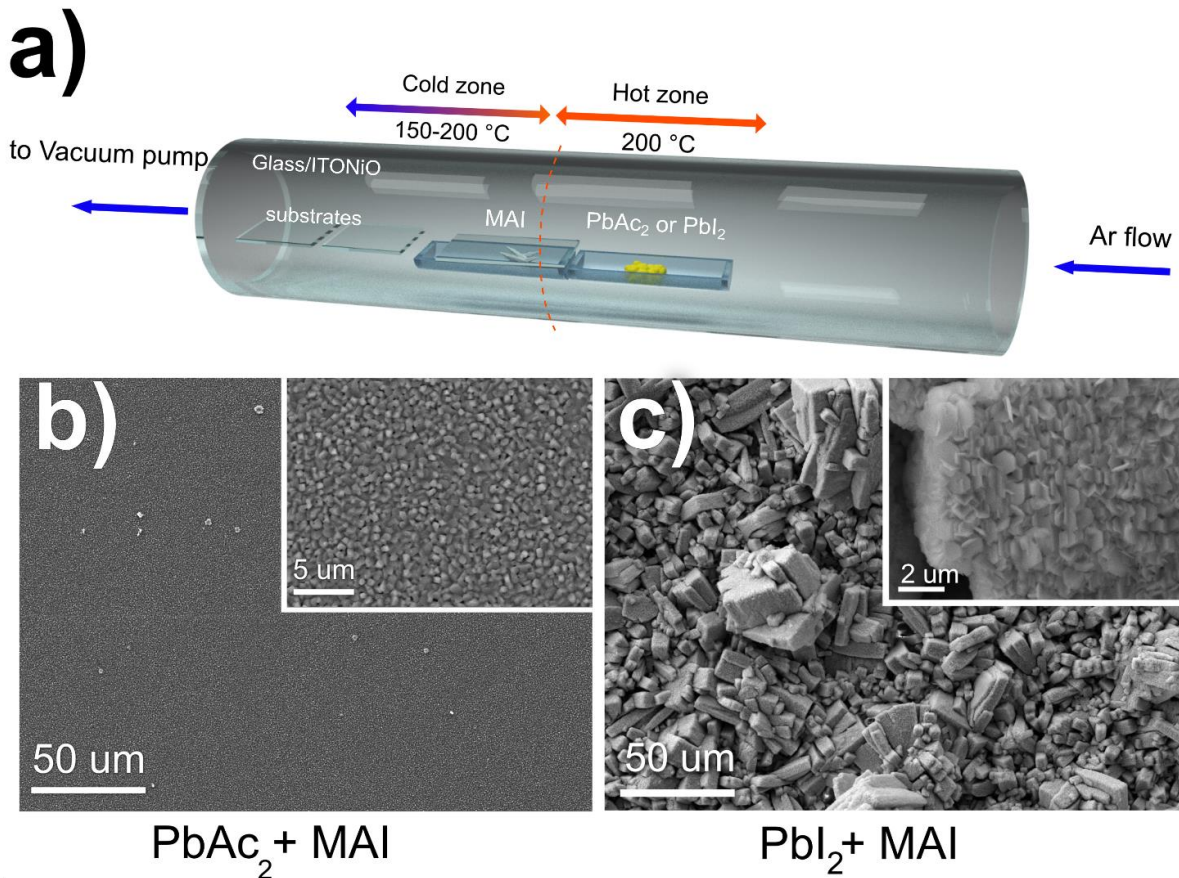


Figure 1. CVD process scheme (a) showing two zones of the furnace and precursor placements for synthesis with PbI_2 we placed it in hot zone and MAI on the cooler side, for the synthesis with PbAc_2 we swapped the precursors to place MAI in the hot zone and PbAc_2 on the cooler side SEM images of the films obtained from lead acetate (b) and lead iodide (c) show different morphology and grain size.

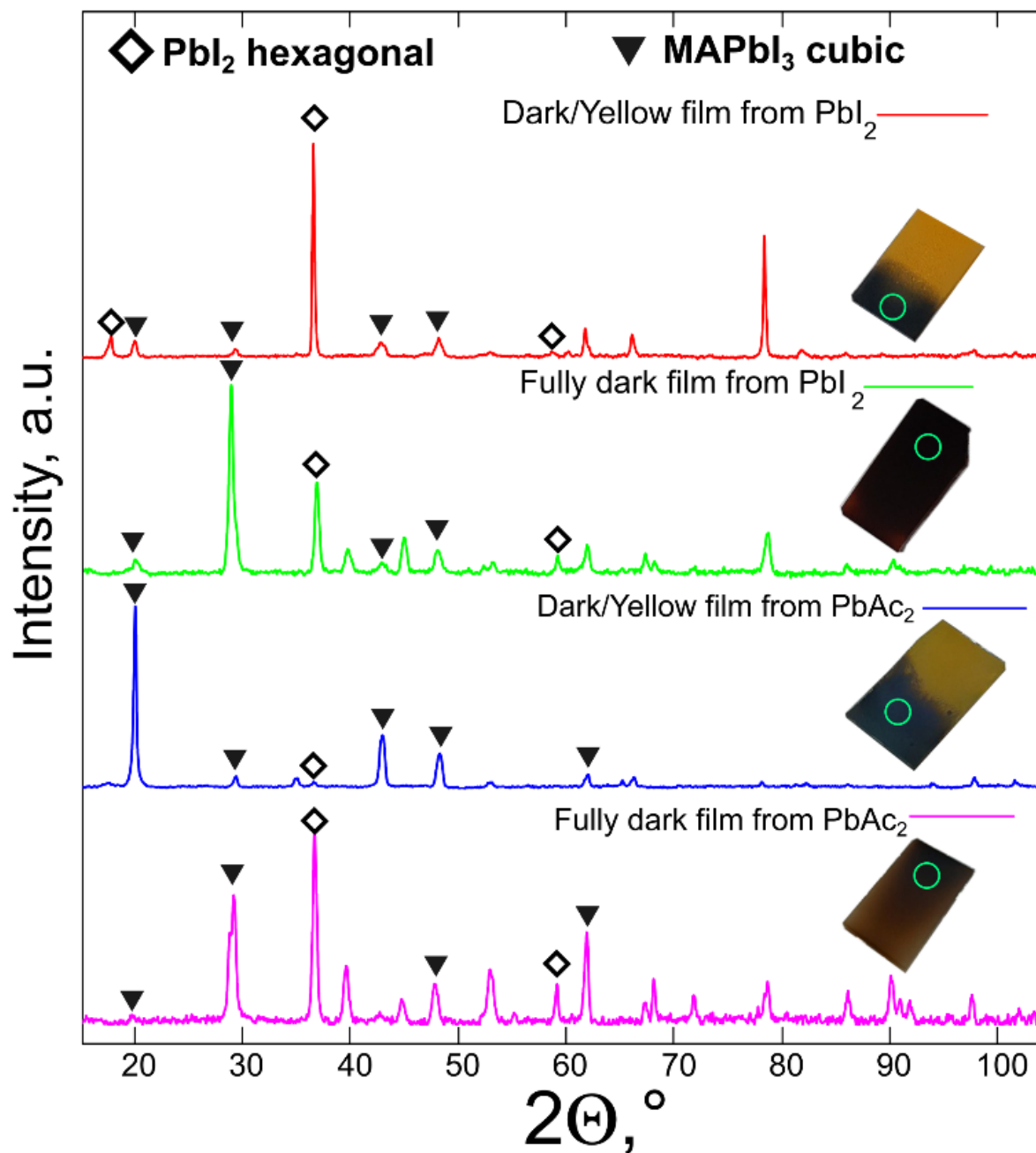


Figure 2. XRD patterns of obtained films on glass from two types of precursors (PbAc_2 and PbI_2). The dark/yellow films were placed closer to the hot zone in the furnace and fully dark films are formed further away from it. The diamond marks hexagonal PbI_2 peaks and triangle marks the peaks of cubic MAPbI_3 phase. The spot from which the pattern was measured is marked with a green circle on all the substrates.

Here the green circles mark the place of the measurement. The two-colored (dark/yellow) film obtained from PbI_2 precursor has both PbI_2 and MAPbI_3 cubic phases, even though the peaks of PbI_2 have higher intensity. Fully dark film obtained with the PbI_2 precursor have higher content of MAPbI_3 but PbI_2 peaks are still present. The most interesting pattern was obtained from the dark part of two-colored (dark/yellow) film when PbAc_2 is used as precursor. As shown in **Fig. 2** (blue line) the peaks of cubic MAPbI_3 phase have very high intensity with almost no additional phases present. That film also has the best morphology and a smooth surface according to SEM data shown in **Fig. 1b**. Fully dark film obtained from PbAc_2 is similar to the dark film from PbI_2 having both PbI_2 and MAPbI_3 phases. We noticed that this dark film from PbAc_2 can change the color to opaque white when exposed to ambient conditions, even though the dark state could be revived by annealing at 100 °C indicating the occurrence of a phase transition. This effect can be explained by the formation of a hydrated $\text{MAPbI}_3 \cdot \text{H}_2\text{O}$ phase in ambient conditions. The rate of hydrated phase formation depends on the amount of unreacted MAI and the degree of conversion of MAPbI_3 to cubic perovskite²⁵.

To confirm the molecular structure of the films, we performed Fourier-transformed infrared (FTIR) spectroscopy (**Fig. 3a**). We compared the spectra of CVD produced films (dark part of dark/yellow substrates) for both PbI_2 and PbAc_2 precursors as well as MAPbI_3 powder obtained by ball milling. The spectra have all the bands for MAPbI_3 described by Abdelmageed et. al.²⁶ On all the spectra the highest intensity band at 906 cm^{-1} is attributed to CH_3NH_3 rocking vibrations, the band at 1460 cm^{-1} is attributed to NH_3 bending vibrations, all the bands in the region from 3040 to 3085 cm^{-1} are attributed to N-H bond stretching. The bands from C-H bond stretching are present but have very low intensity. The main differences of the spectra from the films obtained from PbI_2

and PbAc_2 bands are at 1400 cm^{-1} and 1250 cm^{-1} when the strongest bands at those frequencies are for the films from PbI_2 precursor. The spectrum from PbAc_2 showed the lowest intensity due to low film thickness and was calculated as the difference between the film on glass and pristine glass spectra.

We also analyzed the absorption of the dark films by UV-Vis spectroscopy (**Fig. 3b**). The film obtained from PbAc_2 shows strong absorption band edge at 780 nm, which is typical for MAPbI_3 , on the other hand the film obtained from PbI_2 have the absorption band edge shifted to almost 800 nm. According to X. M. Zhang et al.²⁷ red shift could be due to iodine vacancies and probably partial phase transition from cubic/orthorhombic to trigonal or monoclinic phases We concluded that conditions needed for the formation of a good film from PbAc_2 with cubic MAPbI_3 are well met only at a very narrow area of the furnace.

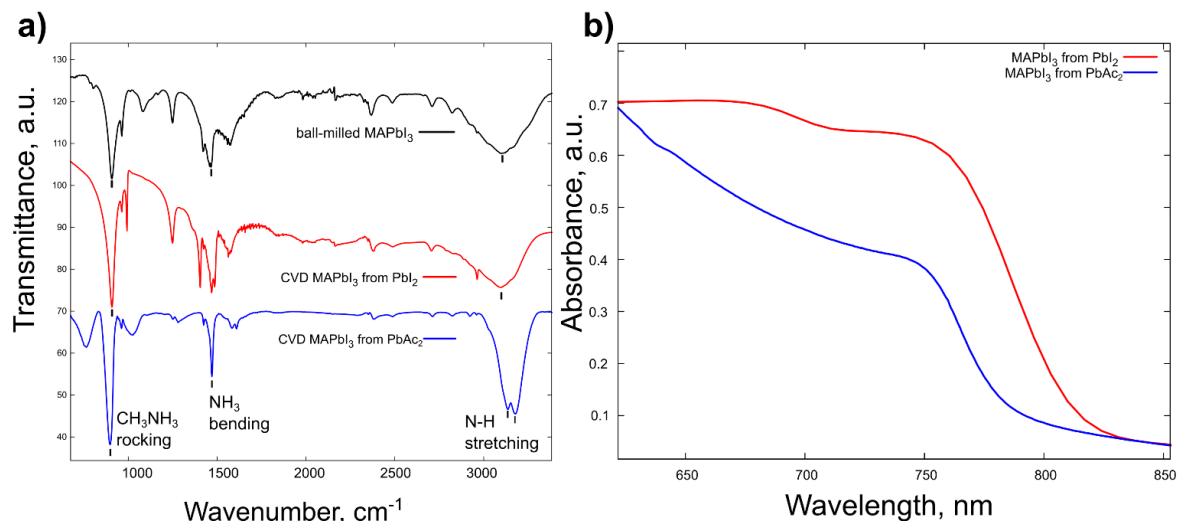


Figure 3. FTIR spectra (a) of ball-milled MAPbI_3 and CVD MAPbI_3 from PbI_2 and PbAc_2 precursors and absorbance spectra for the films from PbI_2 and PbAc_2 showing a shift of absorption band edge from 780 to 800 nm (b)

Owing to the information gathered in these preliminary experiments, we re-design the CVD deposition chamber considering i) substrates placed perpendicular to the gas flow, ii) a larger furnace diameter (50 mm) to increase the properly place the substrate and iii) a second heated zone and separate carrier gas flow rate for the precise control over film deposition conditions. For this scheme, we used 75 sccm flow for PbAc_2 source and 15 sccm for MAI source. The scheme of improved process as well as film and device photographs with PL, UV-Viz data, XRD pattern and SEM images are shown in **Fig. 4**. The optimized deposition scheme increased a number of pixels per single substrate and raised a number of substrates in the single process. Slight shadowing effect for the substrates placed further from the sources does occur, but all the substrates are fully covered with dark MAPbI_3 phase, which is expected for a CVD process²⁸. The films produced in such process have absorbance spectra similar to what was achieved in previous scheme (**fig.4d**) and show a PL peak at 780 nm, which is comparable to what is reported for conventional spin-coated films. Mean thickness of the films is 450 ± 50 nm and should be optimal for device preparation. An XRD pattern of the films have all characteristic peaks of cubic MAPbI_3 (COD: 7225287) and no peaks of PbI_2 phase, that could affect the device performance and increase degradation rate as well. SEM images show lower grain size and smoother looking surface (**Fig. 4f**) if compared to the films produced in the first iteration of our CVD scheme.

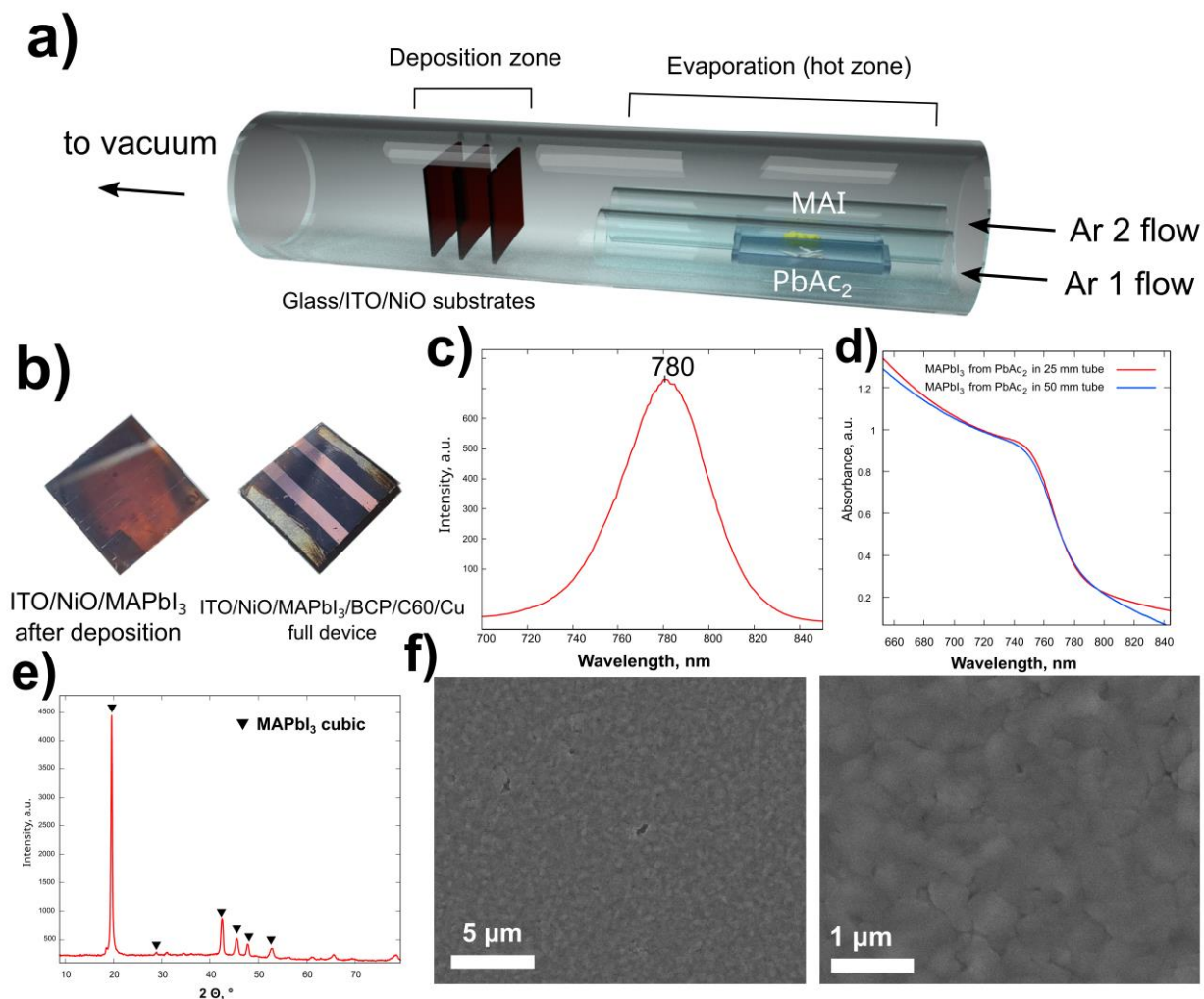


Figure 4. (a) Optimized CVD process scheme, (b) photos of MAPbI₃ film and same film after device assembly, (c) PL spectrum of the film after deposition, (d) Absorbance spectra of MAPbI₃ produced with the first scheme (red) and with optimized scheme (blue), (e) XRD pattern of CVD grown MAPbI₃ film, (f) SEM images of the films produced on bigger substrates in optimized process

After assessment of structural and optical properties of MAPbI₃ thin-films fabricated with CVD approach, we manufactured solar cells with p-i-n architecture. The inverted device structure was realized using the following stack: glass-ITO (pixelated substrate)/NiO_x (hole transporting layer,

20 nm)/perovskite absorber (CVD processing)/C₆₀(electron transport layer, 40 nm)/BCP(hole blocking interlayer, 8 nm)/Copper (cathode, 100 nm). The measurements of the output IV performance were obtained by using the AAA class Solar simulator (Xe Source, 1.5 AM G spectrum calibrated with certified Si cell). Fabricated perovskite solar cells demonstrated interesting performance behavior with strong correlation to the time of light-soaking (LS). As fabricated, devices showed poor performance with open circuit voltage (V_{oc}) = 0.85 V, short circuit current density (J_{sc}) = 0.6 mA/cm², fill factor (FF) = 45 % and power conversion efficiency (PCE) = 0.23 %. By exposing the PSC to continuous light-soaking (light power irradiance density – 100 mW/cm² and heating up to 63±1.5 °C) improved the PCE of PCSs mainly due to an increase of J_{sc} . As it is showed in **fig.5**, the J_{sc} value increased up to 1.39 mA/cm² after 10 minutes of LS and up to 4.71 mA/cm² after 60 minutes. The storage in ambient conditions in the dark also improves the performance. The J_{sc} values of the PSC after dark storage (8 hours) incremented up to 10.8 mA/cm² and showed 5.54 % PCE. This improvement we address to either slow recrystallization or internal stress relaxation of the photoactive layer. After the encapsulation, we observed slightly lower performance, but V_{oc} increased from 0.87 to 0.95 V, which is similar to spin-coated devices of the same configuration. We analyzed the slope of JV curve near V_{oc} point and extracted the values of the series resistance (R_s). The transport properties of “as fabricated” PSC were affected with huge R_s value of 4.27·10² Ohm·cm². Under LS conditions the series resistance reduced up to 6·10¹ Ohm·cm² after 60 minutes. Interestingly, that after dark storage of the devices, series resistance continued the reduction to 2.2·10¹ Ohm cm², while encapsulation processing the value of R_s returned to the 6·10¹ Ohm·cm².

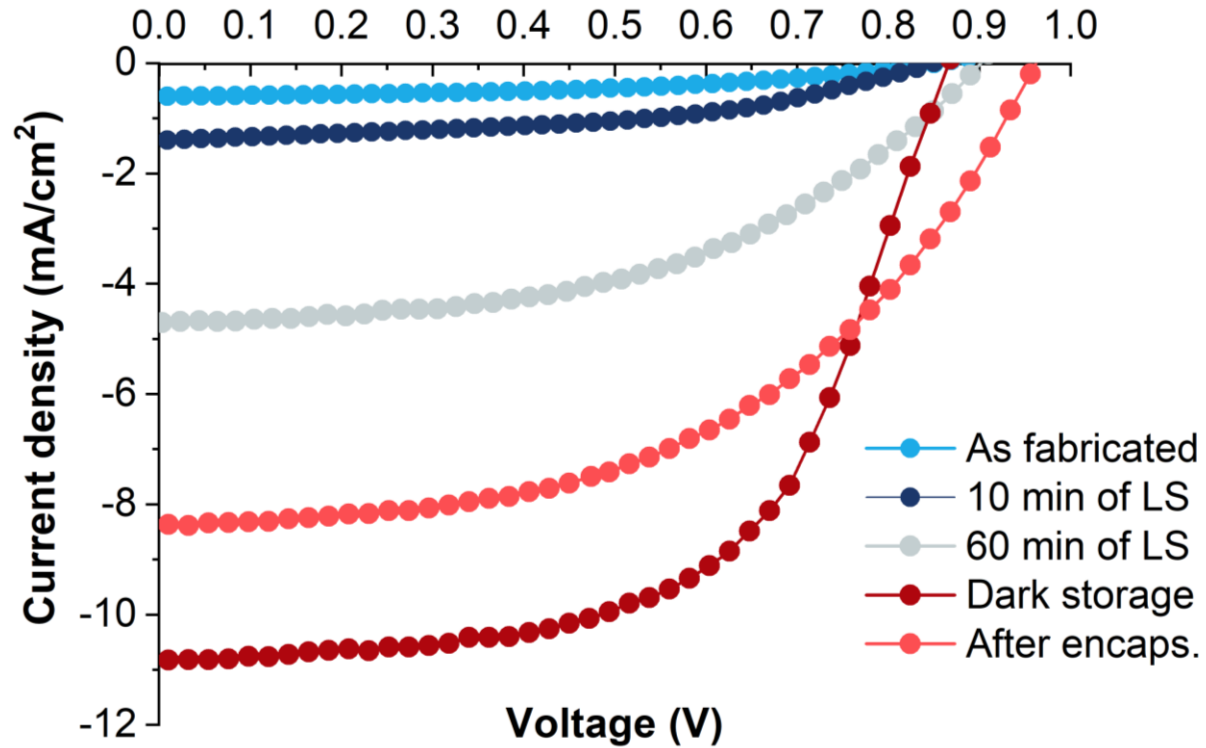


Figure 5. The best JV-curves of devices with CVD produced MAPbI₃ photoactive layer

We observed three main changes of the J-V characteristics induced by the post-fabrication treatments: a) an improvement of the photocurrent during LS; b) the boost of photocurrent after dark storage, and c) the increase of V_{oc} after encapsulation with ultraviolet exposure. The stability of the device performance under continuous light soaking is an important topic for PV and specific features exist for halide perovskite solar cells^{29,30}. The reports on LS highlight the critical role of the light-activated trap-states^{31,32}, self-healing defects^{33,34}, ion migration³⁵ and structural metastability³⁶. Considering methyl-ammonium based perovskites, it is necessary to take into account the relatively low temperature of the photoactive phase transition (55°C)³⁷, which is close to the conditions of the solar cell operation under light illumination and encapsulation. As reported for p-i-n structured PSCs fabricated with solution processing³⁸, the steady state conditions, when device reaches peak power output, requires short period of LS. This process accompanied with

filling of the light activated traps that are represented by shallow and deep-state defects – iodine vacancies³⁹, iodine interstitials⁴⁰, and antisites of iodine with organic cation⁴⁰. In our case, we observed that device require at least 60 minutes to compensate the negative impact of the intrinsic point defects, and probably, finish the phase transition of the absorber film. The improvement of the device performance after dark storage shows, that such condition induces the additional recovery of perovskite layer. As reported by *Cheng et al.*³⁸, the dark storage conditions allows the dissociation of the ionic defects accumulated at the device's interfaces and restoration of the vacancies in the crystal lattice of perovskite. The encapsulation resulted in decrease of the performance originated from the decreased J_{sc} and incremented R_s . We assume that continuous UV-exposure accelerated the formation of the mid-gap light-activated trap and accumulation at the interfaces. The observed changes in the IV performance of the CVD processed PSCs clearly demonstrates that semiconductor properties of the absorber films are meta-stable and sensitive to the light treatment and room temperature storage. The stabilization of the phase transition and control of the defect formation for the CVD perovskite thin-films obviously requires advanced methods for the monitoring of the fabrication process.

Conclusions

In this work, we describe a simple single-step CVD process for the deposition of MAPbI₃ films from solid state precursors both on top of glass and on ITO/NiO substrates. The best films were obtained from lead acetate and methyl-ammonium iodide due to similar melting points. The process we developed produce a smooth film with mean grain size of 0.5 μm and thickness of 450-500 nm. Most of the surface of the film considered cubic phase of MAPbI₃ and can be stable in ambient conditions for several days. The best overall performance of p-i-n MAPbI₃ solar cells of 5.54 % required an implementation of separate control over carrier gas above each of the precursor

powders as well as two-zone heating regime. We also report the formation of metastable dark perovskite-like film at lower deposition temperature. This film undergoes a transition to opaque white film when stored in air, has residual PbI_2 and an excess of iodine according to EDX. When heated to 100 °C this phase quickly returns to dark state. We assume that this phase transition is probably due to transformation from α' to ϵ phase but the temperature is lower due to higher MAI content in the film

Corresponding Author

Dr. Dmitry S. Muratov: muratov@misis.ru

Prof. Aldo DI Carlo aldo.dicarlo@uniforma2.it

Author Contributions

Dmitry S. Muratov: Conceptualization, Methodology, Formal analysis, Data curation, Investigation, Visualization, Writing- Original draft preparation. **Lev Luchnikov:** Methodology, Formal Analysis, Investigation, Visualization. **Artur Ishteev:** Conceptualization, Resources. **Danila Saranin:** Validation, Resources, Data curation, Writing – Review & Editing. **Vladislav Kurichenko:** Methodology, Investigation, Formal analysis. **Evgeny Kolesnikov:** Investigation, Formal analysis, Visualization. **Denis V. Kuznetsov:** Conceptualization, Supervision, Project administration. **Aldo Di Carlo:** Conceptualization, Writing – Original Draft, Review & Editing, Supervision, Project administration, Funding acquisition.

ACKNOWLEDGMENT

The authors gratefully acknowledge the financial support of the Russian Science Foundation (RSF) under grant number 21-19-00853

REFERENCES

- (1) Kazmerski, L. L. Best Research Cell Efficiencies. *Nrel*. 2012, p 1. http://www.nrel.gov/ncpv/images/efficiency_chart.jpg.
- (2) Lu, R.; Liu, Y.; Zhang, J.; Zhao, D.; Guo, X.; Li, C. Highly Efficient (200) Oriented MAPbI₃ Perovskite Solar Cells. *Chemical Engineering Journal* **2022**, *433* (P3), 133845. <https://doi.org/10.1016/j.cej.2021.133845>.
- (3) Rai, M.; Rahmany, S.; Lim, S. S.; Magdassi, S.; Wong, L. H.; Etgar, L. Hot Dipping Post Treatment for Improved Efficiency in Micro Patterned Semi-Transparent Perovskite Solar Cells. *J Mater Chem A Mater* **2018**, *6* (46), 23787–23796. <https://doi.org/10.1039/C8TA09340G>.
- (4) Leyden, M. R.; Ono, L. K.; Raga, S. R.; Kato, Y.; Wang, S.; Qi, Y. High Performance Perovskite Solar Cells by Hybrid Chemical Vapor Deposition. *J Mater Chem A Mater* **2014**, *2* (44), 18742–18745. <https://doi.org/10.1039/c4ta04385e>.
- (5) Xu, F.; Zhang, T.; Li, G.; Zhao, Y. Mixed Cation Hybrid Lead Halide Perovskites with Enhanced Performance and Stability. *J Mater Chem A Mater* **2017**, *5* (23), 11450–11461. <https://doi.org/10.1039/c7ta00042a>.
- (6) Singh, A.; Matteocci, F.; Zhu, H.; Rossi, D.; Mejaouri, S.; Cacovich, S.; Auf Der Maur, M.; Sauvage, F.; Gagliardi, A.; Grätzel, M.; di Carlo, A. Methylamine Gas Treatment Affords Improving Semitransparency, Efficiency, and Stability of CH₃NH₃PbBr₃-Based Perovskite Solar Cells. *Solar RRL* **2021**, *5* (9), 1–10. <https://doi.org/10.1002/solr.202100277>.
- (7) Konstantakou, M.; Perganti, D.; Falaras, P.; Stergiopoulos, T. Anti-Solvent Crystallization Strategies for Highly Efficient Perovskite Solar Cells. *Crystals (Basel)* **2017**, *7* (10), 291. <https://doi.org/10.3390/cryst7100291>.
- (8) Whitaker, J. B.; Kim, D. H.; Larson, B. W.; Zhang, F.; Berry, J. J.; van Hest, M. F. A. M.; Zhu, K. Scalable Slot-Die Coating of High Performance Perovskite Solar Cells. *Sustainable Energy Fuels* **2018**, *2* (11), 2442–2449. <https://doi.org/10.1039/C8SE00368H>.
- (9) Cao, K.; Zuo, Z.; Cui, J.; Shen, Y.; Moehl, T.; Zakeeruddin, S. M.; Grätzel, M.; Wang, M. Efficient Screen Printed Perovskite Solar Cells Based on Mesoscopic TiO₂/Al₂O₃/NiO/Carbon Architecture. *Nano Energy* **2015**, *17*, 171–179. <https://doi.org/https://doi.org/10.1016/j.nanoen.2015.08.009>.

- (10) Tang, M.-C.; Fan, Y.; Barrit, D.; Chang, X.; Dang, H. X.; Li, R.; Wang, K.; Smilgies, D.-M.; Liu, S. (Frank); de Wolf, S.; Anthopoulos, T. D.; Zhao, K.; Amassian, A. Ambient Blade Coating of Mixed Cation Mixed Halide Perovskites without Dripping: In Situ Investigation and Highly Efficient Solar Cells. *J. Mater. Chem. A* **2020**, *8* (3), 1095–1104. <https://doi.org/10.1039/C9TA12890E>.
- (11) Otalora, C.; Botero, M. A.; Mantilla, M. A.; Petit, J. F.; Ospina, R.; Gordillo, G. Hybrid Perovskite Films Deposited by Thermal Evaporation from a Single Source. *Journal of Materials Science: Materials in Electronics* **2021**, *32* (9), 12151–12163. <https://doi.org/10.1007/s10854-021-05844-3>.
- (12) Shin, C.; Jinjoo, Y. L.; Sunbo, P.; Hyeongsik, K.; Sangho, P.; Jung, J.; Yi, J. Current Status of Thin Film Silicon Solar Cells for High Efficiency. **2017**, *5* (4), 113–121. <https://doi.org/https://doi.org/10.21218/CPR.2017.5.4.113>.
- (13) Schmich, E.; Schillinger, N.; Reber, S. Silicon CVD Deposition for Low Cost Applications in Photovoltaics. *Surf Coat Technol* **2007**, *201* (22-23 SPEC. ISS.), 9325–9329. <https://doi.org/10.1016/j.surfcoat.2007.04.089>.
- (14) Wei, X.; Peng, Y.; Jing, G.; Cui, T. Planar Structured Perovskite Solar Cells by Hybrid Physical Chemical Vapor Deposition with Optimized Perovskite Film Thickness. *Jpn J Appl Phys* **2018**, *57* (5). <https://doi.org/10.7567/JJAP.57.052301>.
- (15) Peng, Y.; Jing, G.; Cui, T. High Crystalline Quality Perovskite Thin Films Prepared by a Novel Hybrid Evaporation/CVD Technique. *Materials Research Society Symposium Proceedings* **2016**, *1771*, 187–192. <https://doi.org/10.1557/opl.2015.541>.
- (16) Ioakeimidis, A.; Christodoulou, C.; Lux-Steiner, M.; Fostiropoulos, K. Effect of PbI₂ Deposition Rate on Two-Step PVD/CVD All-Vacuum Prepared Perovskite. *J Solid State Chem* **2016**, *244*, 20–24. <https://doi.org/10.1016/j.jssc.2016.08.034>.
- (17) Gao, Y.; Gu, L.; Fan, Z.; He, J.; Yao, Y.; Tavakoli, M. M.; Reckmeier, C.; Rogach, A. L. Fabrication of Efficient Planar Perovskite Solar Cells Using a One-Step Chemical Vapor Deposition Method. *Sci Rep* **2015**, *5* (1), 1–9. <https://doi.org/10.1038/srep14083>.
- (18) Liu, J.; de Bastiani, M.; Aydin, E.; Harrison, G. T.; Gao, Y.; Pradhan, R. R.; Eswaran, M. K.; Mandal, M.; Yan, W.; Seitkhan, A.; Babics, M.; Subbiah, A. S.; Ugur, E.; Xu, F.; Xu, L.; Wang, M.; Rehman, A. ur; Razzaq, A.; Kang, J.; Azmi, R.; Said, A. A.; Isikgor, F. H.; Allen, T. G.; Andrienko, D.; Schwingenschlögl, U.; Laquai, F.; de Wolf, S. Efficient and Stable Perovskite-Silicon Tandem Solar Cells through Contact Displacement by MgF_x. *Science (1979)* **2022**, *306* (July), 302–306. <https://doi.org/10.1126/science.abn8910>.
- (19) Le, T. S.; Saranin, D.; Gostishchev, P.; Ermanova, I.; Komaricheva, T.; Luchnikov, L.; Muratov, D.; Uvarov, A.; Vyacheslavova, E.; Mukhin, I.; Didenko, S.; Kuznetsov, D.; di Carlo, A. All-Slot-Die-Coated Inverted Perovskite Solar Cells in Ambient Conditions with Chlorine Additives. *Solar RRL* **2022**, *6* (2), 1–11. <https://doi.org/10.1002/solr.202100807>.

- (20) National Center for Biotechnology Information (2022). PubChem Annotation Record for LEAD IODIDE, Source: Hazardous Substances Data Bank (HSDB). <https://pubchem.ncbi.nlm.nih.gov/source/hsdb/636> (accessed 2022-03-04).
- (21) Matsuo Takasuke, S. H. Y. N. Calorimetric and IR Spectroscopic Studies of Phase Transitions in Methylammonium Trihalogenoplumbates (II)†. *Journal of Physics and Chemistry of Solids* **1990**, *51* (12), 1383–1395. [https://doi.org/10.1016/0022-3697\(90\)90021-7](https://doi.org/10.1016/0022-3697(90)90021-7).
- (22) Koza, J. A.; Hill, J. C.; Demster, A. C.; Switzer, J. A. Epitaxial Electrodeposition of Methylammonium Lead Iodide Perovskites. *Chemistry of Materials* **2016**, *28* (1), 399–405. <https://doi.org/10.1021/acs.chemmater.5b04524>.
- (23) Belich, N. A.; Petrov, A. A.; Rudnev, P. O.; Stepanov, N. M.; Turkevych, I.; Goodilin, E. A.; Tarasov, A. B. From Metallic Lead Films to Perovskite Solar Cells through Lead Conversion with Polyhalide Solutions. *ACS Appl Mater Interfaces* **2020**, *12* (18), 20456–20461. <https://doi.org/10.1021/acsami.0c02492>.
- (24) Martínez-Casado, F. J.; Ramos-Riesco, M.; Rodríguez-Cheda, J. A.; Cucinotta, F.; Matesanz, E.; Miletto, I.; Gianotti, E.; Marchese, L.; Matěj, Z. Unraveling the Decomposition Process of Lead(II) Acetate: Anhydrous Polymorphs, Hydrates, and Byproducts and Room Temperature Phosphorescence. *Inorg Chem* **2016**, *55* (17), 8576–8586. <https://doi.org/10.1021/acs.inorgchem.6b01116>.
- (25) Kakekhani, A.; Katti, R. N.; Rappe, A. M. Water in Hybrid Perovskites: Bulk MAPbI₃ Degradation via Super-Hydrous State. *APL Mater* **2019**, *7* (4). <https://doi.org/10.1063/1.5087290>.
- (26) Abdelmageed, G.; Jewell, L.; Hellier, K.; Seymour, L.; Luo, B.; Bridges, F.; Zhang, J. Z.; Carter, S. Mechanisms for Light Induced Degradation in MAPbI₃ Perovskite Thin Films and Solar Cells. *Appl Phys Lett* **2016**, *109* (23). <https://doi.org/10.1063/1.4967840>.
- (27) Zhang, X. M.; Li, J. C.; Wang, X. J.; Wang, F. N.; Du, Y. L.; Su, W. B.; Liu, J.; Li, Y.; Chen, Y. F.; Wang, C. L. Optical Absorption Coefficient Red Shift Effect of Iodine Vacancy in MAPbI₃. *Comput Mater Sci* **2018**, *154* (July), 138–142. <https://doi.org/10.1016/j.commatsci.2018.07.037>.
- (28) Choy, K. L. Chemical Vapour Deposition of Coatings. *Prog Mater Sci* **2003**, *48* (2), 57–170. [https://doi.org/10.1016/S0079-6425\(01\)00009-3](https://doi.org/10.1016/S0079-6425(01)00009-3).
- (29) AG, B.; IS, Z.; S, T.; AF, A.; MM, T.; YS, F.; SI, B.; EY, P.; SY, L.; EZ, K.; KJ, S.; PA, T. Unraveling the Impact of Hole Transport Materials on Photostability of Perovskite Films and P-i-n Solar Cells. *ACS Appl Mater Interfaces* **2020**, *12* (16), 19161–19173. <https://doi.org/10.1021/ACSAMI.0C01027>.
- (30) Zhang, Y.; Wang, P.; Yu, X.; Xie, J.; Sun, X.; Wang, H.; Huang, J.; Xu, L.; Cui, C.; Lei, M.; Yang, D. Enhanced Performance and Light Soaking Stability of Planar Perovskite Solar Cells Using an Amine-Based Fullerene Interfacial Modifier. *J Mater Chem A Mater* **2016**, *4* (47), 18509–18515. <https://doi.org/10.1039/C6TA08992E>.

- (31) Sherkar, T. S.; Momblona, C.; Gil-Escrig, L.; Ávila, J.; Sessolo, M.; Bolink, H. J.; Koster, L. J. A. Recombination in Perovskite Solar Cells: Significance of Grain Boundaries, Interface Traps, and Defect Ions. *ACS Energy Lett* **2017**. <https://doi.org/10.1021/acsenerylett.7b00236>.
- (32) Hoke, E. T.; Slotcavage, D. J.; Dohner, E. R.; Bowring, A. R.; Karunadasa, H. I.; McGehee, M. D. Reversible Photo-Induced Trap Formation in Mixed-Halide Hybrid Perovskites for Photovoltaics. *Chem Sci* **2015**. <https://doi.org/10.1039/c4sc03141e>.
- (33) Li, Z.; Xiao, C.; Yang, Y.; Harvey, S. P.; Kim, D. H.; Christians, J. A.; Yang, M.; Schulz, P.; Nanayakkara, S. U.; Jiang, C.-S.; Luther, J. M.; Berry, J. J.; Beard, M. C.; Al-Jassim, M. M.; Zhu, K. Extrinsic Ion Migration in Perovskite Solar Cells. *Energy Environ Sci* **2017**, *10* (5), 1234–1242. <https://doi.org/10.1039/C7EE00358G>.
- (34) de Bastiani, M.; Aydin, E.; Allen, T.; Walter, D.; Fell, A.; Peng, J.; Gasparini, N.; Troughton, J.; Baran, D.; Weber, K.; White, T. P.; de Wolf, S. Interfacial Dynamics and Contact Passivation in Perovskite Solar Cells. *Adv Electron Mater* **2019**, *5* (1), 1800500. <https://doi.org/10.1002/aelm.201800500>.
- (35) Li, Z.; Li, B.; Wu, X.; Sheppard, S. A.; Zhang, S.; Gao, D.; Long, N. J.; Zhu, Z. Organometallic-Functionalized Interfaces for Highly Efficient Inverted Perovskite Solar Cells. *Science* (1979) **2022**, *376* (6591), 416–420. <https://doi.org/10.1126/science.abm8566>.
- (36) Fu, Q.; Tang, X.; Huang, B.; Hu, T.; Tan, L.; Chen, L.; Chen, Y. Recent Progress on the Long-Term Stability of Perovskite Solar Cells. *Advanced Science*. 2018. <https://doi.org/10.1002/advs.201700387>.
- (37) Whitfield, P. S.; Herron, N.; Guise, W. E.; Page, K.; Cheng, Y. Q.; Milas, I.; Crawford, M. K. Structures, Phase Transitions and Tricritical Behavior of the Hybrid Perovskite Methyl Ammonium Lead Iodide. *Sci Rep* **2016**. <https://doi.org/10.1038/srep35685>.
- (38) Cheng, Y.; Liu, X.; Guan, Z.; Li, M.; Zeng, Z.; Li, H. W.; Tsang, S. W.; Aberle, A. G.; Lin, F. Revealing the Degradation and Self-Healing Mechanisms in Perovskite Solar Cells by Sub-Bandgap External Quantum Efficiency Spectroscopy. *Advanced Materials* **2021**, *33* (3). <https://doi.org/10.1002/adma.202006170>.
- (39) Polyakov, A. Y.; Smirnov, N. B.; Shchemerov, I. v.; Saranin, D. S.; Le, T. S.; Didenko, S. I.; Kuznetsov, D. v.; Agresti, A.; Pescetelli, S.; Matteocci, F.; di Carlo, A. Trap States in Multication Mesoscopic Perovskite Solar Cells: A Deep Levels Transient Spectroscopy Investigation. *Applied Physics Letters*. American Institute of Physics Inc. December 24, 2018. <https://doi.org/10.1063/1.5053845>.
- (40) Vasilev, A. A.; Saranin, D. S.; Gostishchev, P. A.; Didenko, S. I.; Polyakov, A. Y.; di Carlo, A. Deep-Level Transient Spectroscopy of the Charged Defects in p-i-n Perovskite Solar Cells Induced by Light-Soaking. *Optical Materials: X* **2022**, *16*, 100218. <https://doi.org/10.1016/j.omx.2022.100218>.